

Drying of Compact and Porous NCM Cathode Electrodes in Different Multilayer Architectures: Influence of Layer Configuration and Drying Rate on Electrode Properties

Julian Klemens,* David Burger, Luca Schneider, Sandro Spiegel, Marcus Müller, Nicole Bohn, Werner Bauer, Helmut Ehrenberg, Philip Scharfer, and Wilhelm Schabel

Porous, nanostructured particles ensure the wetting of electrolyte up to the particle core and shortened diffusion paths, which is relevant not only for lithium-ion batteries but also for postlithium systems like sodium-ion batteries. The porous structure leads to a high C-rate capability. However, compared to conventional compact NCM, porous NCM shows a reduced adhesion force but no or only slight negative influence on C-rate capability by binder migration at higher drying rates. Herein, a multilayer concept is used to increase the adhesion force with equal or better electrochemical performance compared to single-layer electrodes. Compact particles of high volumetric energy density and porous particles with high C-rate capability are combined in a simultaneously coated multilayer electrode. Multilayers with compact NCM toward the current collector and porous NCM with reduced binder content toward the separator side show an about 16-times higher adhesion force at lower drying rate and an about ten-times higher adhesion force at increased drying rate compared to electrodes produced of porous NCM only. The specific discharge capacity of the multilayers is increased by 88% at the lower and 67% at the higher drying rate for a discharge rate of 3C compared to a single layer with compact NCM.

produced from conventional active materials when the compact material is milled and spray dried into secondary particles with an internal, accessible porosity. The open porosity ensures wetting of the electrolyte up to the particle core and shortens the diffusion paths. As given in the literature, the diffusion coefficient in the electrolyte phase (LP30, e.g., $10^{-6} \text{ cm}^2 \text{ s}^{-1}$)^[4,5] is much higher compared to the solid phase (NCM, e.g., 10^{-10} – $10^{-11} \text{ cm}^2 \text{ s}^{-1}$).^[6,7] A similar hierarchical particle concept is used for cathode active materials of sodium-ion batteries (sodium–vanadium phosphate, NVP) to enable the electrolyte filling up to the core of the material.^[8–11]

However, electrodes with porous particles exhibit a lower adhesion force compared to electrodes produced of compact particles at the same mass fraction of binder in the electrodes. The solvent, and in particular the dissolved binder, penetrates the particles (intraparticle porosity) during slurry production and remains

there after drying.^[1] This binder component is prevented to contribute to the adhesion to the current collector.^[1,3] The penetration and fixation of the binder within the particles result in less clogging of the pores in the pore network, which is responsible for the approximately constant C-rate capability^[1] and tortuosity^[7] at higher drying rates. In electrodes with compact particles, the binder and conductive additives are located only in the pore network between the active material particles (interparticle porosity)^[1,3] and is referred to as the carbon binder domain (CBD).

With increasing drying rate, the mobile binder fraction migrates in the interparticle pore network and leads to an accumulation at the top of the electrode and a depletion of binder at the current collector. Binder migration was observed for anodes and cathodes as well as for aqueous and solvent-based electrodes.^[1,12–26] An accumulation of binder toward the separator side increases the ionic and electrical resistance and reduces the C-rate capability.^[1,17,23,25] The ionic resistance is increased compared to electrodes with a homogeneous binder distribution or electrodes with a lower binder content.^[23,27,28]

The adhesion force is reduced at increasing drying rate and can possibly lead to delamination of electrode films.^[12,20,25,26,29] Electrodes produced of porous, nanostructured particles with an

1. Introduction

The use of porous, nanostructured particles in electrodes for lithium-ion batteries (LIB) can significantly improve their electrochemical performance.^[1–3] Porous particles can be

J. Klemens, D. Burger, S. Spiegel, P. Scharfer, W. Schabel
Thin Film Technology (TFT)
Karlsruhe Institute of Technology (KIT)
Straße am Forum 7, D-76131 Karlsruhe, Germany
E-mail: julian.klemens@kit.edu

L. Schneider, M. Müller, N. Bohn, W. Bauer, H. Ehrenberg
Institute for Applied Materials (IAM) – Energy Storage Systems (ESS)
Karlsruhe Institute of Technology (KIT)
Hermann-von-Helmholtz-Platz 1, 76344 Eggenstein-Leopoldshafen,
Germany

 The ORCID identification number(s) for the author(s) of this article can be found under <https://doi.org/10.1002/ente.202300267>.

© 2023 The Authors. Energy Technology published by Wiley-VCH GmbH. This is an open access article under the terms of the Creative Commons Attribution License, which permits use, distribution and reproduction in any medium, provided the original work is properly cited.

DOI: 10.1002/ente.202300267

increased specific surface area also show binder migration at increasing drying rate, but with much less or no negative influence on the specific discharge capacity. This is because the binder is not highly concentrated between the particles clogging the pores, but a certain amount of binder is fixed in the particles and does not migrate during drying.^[1]

To improve electrode properties and, in particular, the adhesion force, while maintaining or improving C-rate capability, multilayer electrodes can be produced with different formulations and particle morphologies.^[13,19,30–35] For aqueous graphite electrodes made with carboxymethyl cellulose (CMC) and styrene–butadiene–rubber (SBR), it was shown that the adhesion force and the C-rate capability can be improved by a multilayer structure of the electrode. Electrodes made with simultaneously applied slurries of different SBR–binder content at the same total binder content, same wet and dry film thickness and viscosity were investigated at KIT.^[13] The improvement was attributed to the concentration of the total amount of SBR in the bottom layer after the coating process, which is presumably homogeneously distributed over the entire electrode during drying by capillary transport.^[13] For cathodes with the one-component binder polyvinylidene fluoride (PVDF) and the solvent *N*-methyl-2-pyrrolidone (NMP), a similar approach of multilayers with an increased binder content in the bottom layer and a decreased content in the top layer was investigated.^[34] In contrast to the aqueous multilayers, binder migration at increased drying temperature resulted in an accumulation at the top and a depletion of binder at the bottom of the electrode.^[34] For both binder systems, the distinct influence of viscosity, layer thickness ratio of top and bottom layer, and the solid content on binder migration has not been clarified and may vary depending on the binder–solvent system used.

It is not known from the literature how binder migration in multilayer electrodes behaves during drying of electrodes with different particle morphologies, binder contents, and drying rates. The aim of this study is to better understand the processing and, in particular, the drying behavior of simultaneously coated multilayer electrodes depending on the active particles and the overall binder content. The multilayer electrodes are intended to improve the properties of the electrodes compared to single-layer electrodes. They should improve both the adhesion of the active material to the collector for electrodes produced of porous, nanostructured particles and the C-rate capability compared to electrodes produced with compact active material.

The influence of multilayer electrodes produced of two different particle morphologies on the adhesion force, electrical and ionic resistance, and the C-rate capability is investigated. This study is intended to extend the previous understanding of multilayer electrode processing and the use of porous, nanostructured battery active materials for LIB and postlithium batteries.

2. Results and Discussion

Multilayer electrodes were produced using two particle systems with different layer configurations and binder contents. For the multilayer coating, an intermixing of the slurries during simultaneous coating is to be avoided. Therefore, slurries are adjusted, that the viscosity of the upper layer has a lower viscosity than the lower layer by reducing the binder content, which also reduces the share of passive materials.

2.1. Multilayer Configuration

Porous NCM622 particles were produced using the same procedure as presented in the literature.^[1–3] An overview of the particle properties can be found in **Table 1**. The density of the porous NCM with the intergranular porosity is calculated with Equation (1) (see Experimental Section).

According to the literature, it is known that because of the open-porous structure of the particles, both the binder and the solvent penetrate into the particles during slurry preparation.^[1,3] Due to the internal porosity ($\epsilon_{\text{porous particles}} = 33\%$), other effective volume fractions act in the slurry. In contrast to the binder solution, the conductive additives remain in the outer pore volume around the active particles, which increases the flow resistance. For the same composition, mixing procedure, and solid content a slurry containing porous particles shows a much higher viscosity compared to a slurry with compact particles (Figure S1, Supporting Information). Therefore, the slurries for this study were prepared such that the dry electrode with the compact particles had a PVDF content of 4.5 wt% and the electrodes with the porous particles had a reduced binder content of 3 wt%. By that, the binder content was adjusted to achieve an overall reduction of the binder content compared to the single-layer configuration. The slurries were prepared with the same solid content (55 wt% solids) and mixing procedure (see Experimental Section). The rheological behavior of the slurries is shown in **Figure 1**.

With a reduced binder content of 3 wt%, the viscosity of NCM622-porous has been adjusted to be in the range and below the viscosity curve of the NCM622-compact (see Figure 1). With this flow behavior of the two slurries, we assume that intermixing will not occur during simultaneous coating.

These two slurries were used to produce electrodes with different multilayer architectures. The lower layer in the multilayer electrodes always consists of compact particles and the upper layer of porous particles. Layer configurations with different layer thickness proportions of layers with compact and porous particles are produced. Thus, the dried multilayer electrodes consist either of a higher proportion with porous particles (ML–2/3 porous) in the upper layer or a higher proportion with compact particles (ML–1/3 porous) in the lower layer. **Figure 2** shows the

Table 1. Overview of the particle size, specific surface area, density (measured by gas pycnometry), and internal porosity of the particles.

Name	Secondary particle diameter x_{50} [μm]	Specific surface area [$\text{m}^2 \text{g}^{-1}$]	Density [g cm^{-3}]	Open particle porosity [%]	Envelope density [g cm^{-3}]
NCM622-compact	9.5	0.7	4.64	–	4.64
NCM622-porous	8.4	3.5	4.56	33	3.06

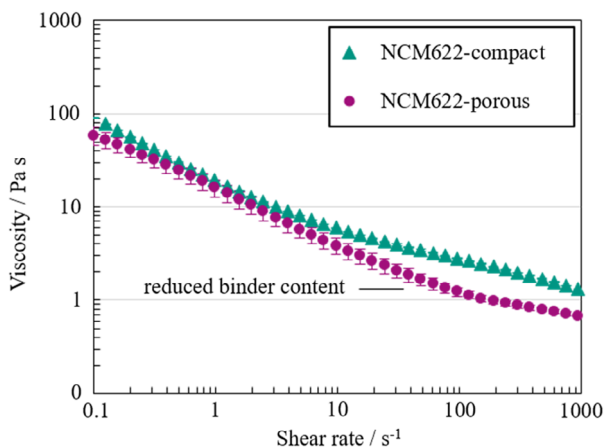


Figure 1. Viscosity of slurries with compact particles (NCM622-compact, green triangles) and porous, nanostructured particles (NCM622-porous, red dots) as a function of the shear rate at 25 °C. The binder content of the NCM622-porous slurry was reduced to avoid intermixing of the slurries during simultaneous coating. The slurries have the same solid content of 55 wt%.

two single layers (SL compact, SL porous) and, as an example, the multilayer electrode with a larger proportion of porous particles in the upper layer (ML 2/3 porous).

As expected after reducing the viscosity by adjusting the binder content for the slurry with the porous particles, no intermixing was observed for the multilayer electrodes in Figure 2. This finding was expected, since the viscosity was adjusted via the binder content that the viscosity of the slurry of the upper layer was lower than the bottom layer.

Since the coating thickness has an influence on the drying and the adhesion force, the electrodes were produced with approximately the same dry film thickness (Table 2). An overview of the dry film thickness, area weight, and electrode porosity of the single- and multilayer electrodes is given in Table 2.

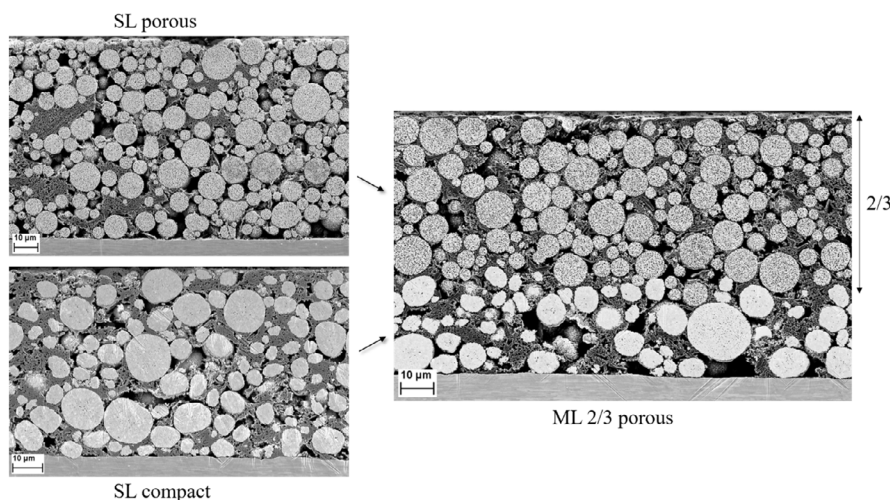


Figure 2. SEM cross-sectional images of a dried single-layer electrode with porous particles (SL porous), a single-layer electrode with compact particles (SL compact), and a multilayer electrode with a dominating proportion of porous particles in the top layer (ML 2/3 porous) as an example. The multilayer electrode shows that no intermixing of the two slurries with the different particles occurred during the coating process.

Table 2. Dry film thickness, area weight, electrode porosity, and interparticle porosity of single- and multilayer electrodes.

Name	Dry film thickness [μm]	Area weight [g m^{-2}]	Electrode porosity [%]	Interparticle porosity [%]
SL compact	94.1 ± 1.2	220.0 ± 4.1		42.8 ± 0.7
SL porous	97.3 ± 2.2	160.3 ± 3.9	60.0 ± 0.1	43.6 ± 0.1
ML 1/3 porous	100.6 ± 1.9	201.1 ± 0.7	51.2 ± 0.7	45.9 ± 0.8
ML 2/3 porous	101.7 ± 1.6	188.1 ± 1.1	54.9 ± 0.5	44.1 ± 0.6

The density of NCM622-porous particles of 4.56 g cm^{-3} (Table 1) was used to calculate the electrode porosity (see Experimental Section, Equation (1) and (2)). In addition, the porosity between the particles (interparticle porosity) is shown for the electrodes containing porous particles (see Experimental Section, Equation (1)–(3)).

Due to the open porosity of the porous particles ($\epsilon_{\text{porous particles}} = 33\%$) in the single-layer (SL porous) and the multilayer electrodes, the electrode porosity is increased compared to the single layer with compact particles. Ignoring the internal porosity of the porous particles, the porosity between the particles (interparticle porosity) for all electrodes is about 44%. This matches the presumption that the electrodes with porous particles would have the same interparticle porosity compared to electrodes with compact particles, since the particles have a similar particle size and the electrode composition contains the same proportions of conductive additives. The area weight of the multilayer electrode is increased compared to the area weight of the single-layer electrode with porous particles due to the combination with the compact particles.

2.2. Adhesion

The single- and multilayer electrodes were produced under isothermal drying conditions in a customized coating and drying apparatus.^[12,17,21] The dryer as well as the temperature-controlled

coating plate were set to the temperature that a drying electrode would take as the adiabatic wet bulb temperature if dried in a convective roll-to-roll coating and drying machine. An isothermal drying temperature (film temperature) of 61 °C was set at the lower drying rate of $0.75 \text{ g m}^{-2} \text{ s}^{-1}$ and a temperature of 81 °C at the three times higher drying rate of $2.25 \text{ g m}^{-2} \text{ s}^{-1}$ with a heat transfer coefficient of $80 \text{ W m}^{-2} \text{ K}^{-1}$. It is considered, that drying rates higher than $1.5 \text{ g m}^{-2} \text{ s}^{-1}$ are relevant for industrial manufacturing.^[21] With the area weights shown in Table 2 and the solids content of 55 wt%, the drying rate increase results in a reduction of drying time from $207 \pm 33 \text{ s}$ to $69 \pm 11 \text{ s}$.

The adhesion force between the current collector and the coating (see Experimental Section) of the single- and multilayer electrodes was investigated as an indicator for binder migration at increasing drying rate (Figure 3). Cohesion failures due to the application of two different layers with different particles and binder contents did not occur.

The adhesion force of the two single-layer electrodes with porous particles shows very low values of $2.55 \pm 0.45 \text{ N m}^{-1}$, as expected from the literature.^[1,3] As a comparison, an electrode with compact particles and an identical binder content of 3 wt% would show an adhesive force of about 28 N m^{-1} for the lower drying rate. The adhesion force of the single layer with compact particles decreases with increasing drying rate by adaption of the isothermal drying temperature, which is in agreement with the literature for both solvent- and water-based anodes and cathodes.^[1,12,21,25,26]

For both layer configurations and both drying rates, the adhesion force of the multilayer electrodes decreases, although the adhesion force is higher with a larger proportion of compact particles (ML 1/3 porous) in the lower layer. The adhesion force of the multilayer electrode (ML 1/3 porous) is increased by a factor of 16 at lower drying rate and by a factor of 10 at higher drying

rate compared to the single-layer electrode with porous particles. The result that the adhesion force of the multilayers is increased compared to the single layer with only porous particles was expected, since electrodes with compact particles generally show a higher adhesion force.^[1,3] However, it has been expected that the adhesion force of the multilayers would be higher in accordance with the absolute values of the single layers with compact particles. The finding, that the adhesion force of the multilayers would be higher in accordance with the absolute values of the single layers with compact particles. The finding, that the adhesion force of the single-layer electrode with a binder content of 4.5 wt% is not achieved with the multilayer configuration, could be explained by the total binder content in the electrodes. Figure 4 shows the adhesion force as a function of the overall binder content for electrodes containing only compact particles. The overall binder content results from the mass ratio and the binder content of each layer.

An exponential relationship is observed between the adhesion force and the overall binder content in the single- and multilayer electrodes, with the bottom layer consisting of compact active material. With increasing drying rate, this relationship shifts to a lower adhesion force. The exponential behavior may be explained by a superposition of proffered amount of binder and the intensity of binder migration, leading to a certain amount of contact between the current collector and the electrode layer. Increasing interactions of the binder with the current collector due to a higher amount of binder lead to an exponentially increasing adhesion force.

In the drying rate range investigated, the adhesion force of the single layer with compact particles (4.5 wt% PVDF) decreases by about 30%. In contrast to the single layers with compact particles, the adhesion force of the multilayers drops with increasing drying rate by 56% for the multilayer with 1/3 porous particles (4 wt% overall binder content) and 62% for the multilayer with 2/3 porous particles (3.5 wt% overall binder content). As shown,

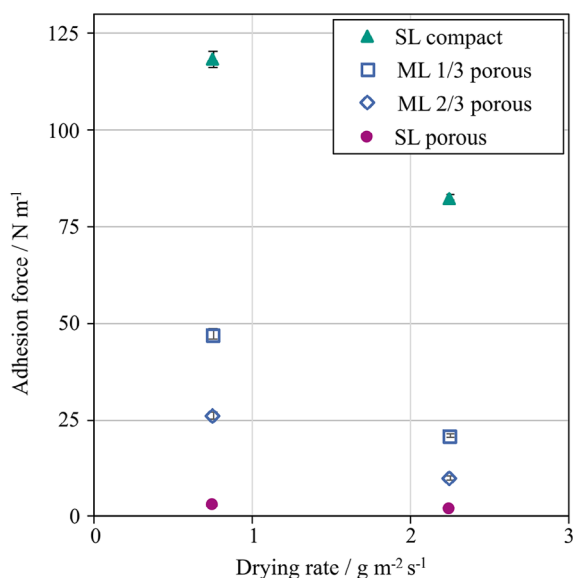


Figure 3. Adhesion force (90° peel test) of single-layer electrodes (SL compact: green triangles, SL porous: red dots) and multilayer electrodes (ML 1/3 porous: blue squares, ML 2/3 porous: blue rhombus) at a lower drying rate of $0.75 \text{ g m}^{-2} \text{ s}^{-1}$ (61 °C isothermal drying temperature) and a higher drying rate of $2.25 \text{ g m}^{-2} \text{ s}^{-1}$ (81 °C isothermal drying temperature).

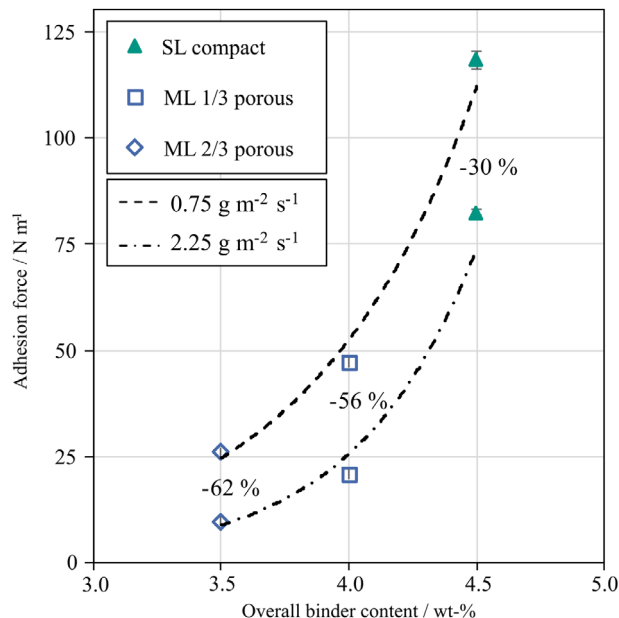


Figure 4. Adhesion force (90° peel test) of single-layer electrodes (SL Compact: green triangles) and multilayer-cathode electrodes (ML 1/3 porous: blue squares, ML 2/3 porous: blue rhombus) as a function of the overall binder content in the electrodes.

the absolute value of the adhesion force decreases relatively more with lower total binder content of the electrode. This could also be described by the interaction of the binder amount at the current collector. If comparatively less binder is present in the formulation, binder migration leads to a stronger relative decrease in adhesion force.

As previously described, it was expected that the adhesion force of the multilayer is more oriented toward the adhesion force of the lower layer. The result that the behavior is dependent on the overall binder content in the electrode, although a binder gradient is imposed by the multilayer coating, could be explained by a diffusional concentration balancing process of the binder before the capillary transport occurs. However, intermixing of the slurries due to a mixing flow during coating was excluded, since the distribution of active particles in the cross section shows a clear separation of the two particle morphologies (Figure 1). A gradual alignment of the PVDF concentration in NMP by diffusion is conjecturable, as the homogenous shrinkage of a polymer film is based on diffusional solvent transport in the film.^[36,37] This reveals an important insight for the manufacturing of multilayers with PVDF/NMP.

In contrast, a linear relationship between the binder content in the bottom layer and the resulting adhesion force of the multilayer was found for aqueous anodes with the two-component CMC/SBR system.^[13]

The results in this study and the data from the literature indicate that there are different options for different binder systems to optimize electrode properties. For the two-component system of CMC/SBR, for example, it is possible to adjust the binder content (SBR) with only slight effects on the viscosity.^[13] For the one-component system with PVDF, this is not possible and there are less degrees of freedom for the formulation.

2.3. Resistivity

Resistivity measurements were carried out to investigate the influence of the coating configuration on the electrical conductivity as a function of the drying rate. The resistivity for the single- and multilayer electrodes with increasing drying rate is shown in Figure 5.

For all electrodes, the electrical resistivity increases with increasing drying rate, which could be related to the binder migration in all layers. The resistivity is significantly higher for the porous single layers, which is consistent with the literature.^[1,3] An electrode with compact particles in contact with the current collector and a binder content of 3 wt% (like the SL porous electrodes) shows a resistivity of $\approx 7 \Omega \text{ m}$ for the lower drying rate. The higher resistivity for electrodes with porous particles is attributed to the higher porosity of the electrodes with porous particles (Table 2). Since the binder is fixed in the particles, it contributes less to contact (lower adhesion force) the current collector. Assuming that the binder in the pore network outside the particles becomes conductive to some extent due to the conductive carbon black, lower contacting results in lower electrical connection to the current collector.^[1,7] The measured resistivity for the multilayer electrodes is more oriented toward the resistivity of the single layer with compact particles. This suggests that the measurement method between two plates is

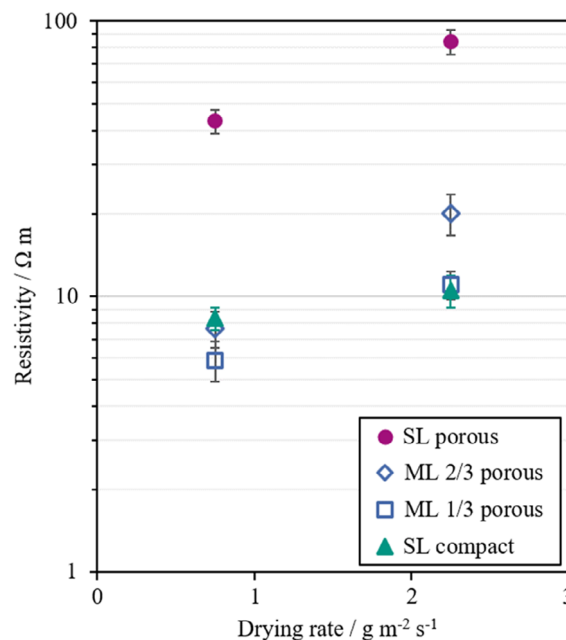


Figure 5. Resistivity of non-calendered single-layer (SL compact: green triangles, SL porous: red dots) and multilayer (ML 1/3 porous: blue squares, ML 2/3 porous: blue rhombus) electrodes as a function of drying rate.

sensitive for the contact resistance between the dry coating and the current collector in the lower area of the electrode. The contact resistances seem to exceed the electrical resistance in the electrode layer and may match with the mechanical amount of contact indicated by the measurement of adhesion force (Figure 3).

Therefore, for electrodes where compact particles are in contact with the current collector, the resistivity increases more with lower total binder content. The resistivity increases by 26% for the single-layer electrode SL compact (4.5 wt% PVDF), 88% for multilayer ML 1/3 porous (4 wt% PVDF), and 160% for multilayer ML 2/3 porous (3.5 wt% PVDF). This is consistent with the observations from Section 2.2. Again, it can be seen that the property of electrodes with a lower total binder content is relatively more influenced by the influence of the binder migration due to a higher drying rate.

2.4. Electrochemical Characterization

The influence of the construction of multilayer electrodes and faster drying on the cell performance are investigated by coin-cell tests with increasing C-rate. Noncalendered electrodes as for the measurements of the adhesion force (Figure 3 and 4) and electrical resistance (Figure 5) are used for the cell tests. Figure 6 shows the specific capacity of the single- and multilayers dried at the lower drying rate.

It is shown that the single- and multilayer electrodes containing porous particles have higher specific discharge capacities compared to the single layer with compact particles, especially at higher C-rates. At 3C, the discharge capacity of the single-layer electrode with porous particles is about 118%, the multilayer ML

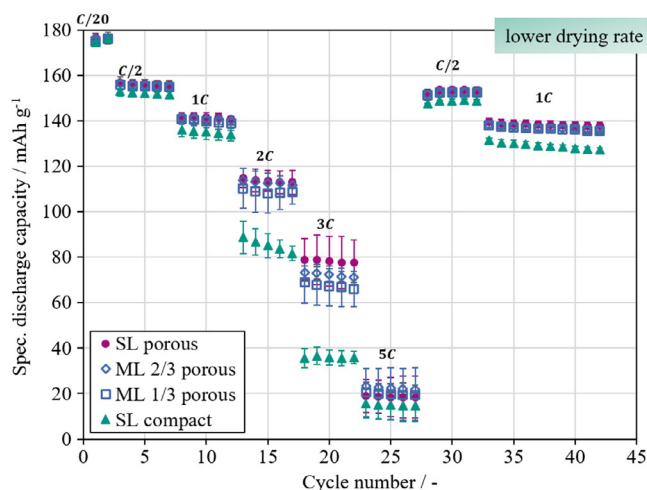


Figure 6. Specific discharge capacities of half cells with non-calendered single-layer (SL compact: green triangles, SL porous: red dots) and multi-layer electrodes (ML 1/3 porous: blue squares, ML 2/3 porous: blue rhombus) at a constant drying rate of $0.75 \text{ g m}^{-2} \text{ s}^{-1}$.

2/3 porous about 101%, and the multilayer ML 1/3 porous is about 88% higher than the discharge capacity of the single-layer electrode with compact particles. It can be suggested that the C-rate capability increases with the proportion of porous particles. It is excluded that a reduction of the binder fraction for an electrode with compact particles leads to such an increase in the C-rate stability. In the Supporting Information S2, a comparison of the SL compact with a single layer of compact particles and reduced binder content is shown. For example, at 3 C, the discharge capacity is about 42 mAh g^{-1} .

Remarkably, even a small amount of porous particles in the multilayer ML 1/3 porous leads to a large increase in specific capacity at higher C-rates compared to the single-layer electrode with compact particles. It should be mentioned that the standard deviations partially overlap and the SL porous- and the multilayer electrodes have a reduced binder content. The use of the porous particles and the reduction of the binder content result in a lower ionic resistance determined by impedance measurements (Table S1, Supporting Information). Furthermore, the multilayer electrodes show a lower electrical resistivity compared to the single layer of porous particles. Together, these effects could result in a positive impact on the electrochemical performance of the multilayers.

Figure 7 shows the discharge capacities at a drying rate of $2.25 \text{ g m}^{-2} \text{ s}^{-1}$.

The C-rate capability can be improved at higher drying rates using porous particles only or the multilayer architectures. Compared to the SL compact, the specific discharge capacities of the SL porous show an increase of about 161% at a discharge rate of 3 C, pointing out the advantage of the porous particles, especially at high drying rates. Subsequently the multilayer ML 2/3 porous provides an 88% increase compared to the SL compact but a lower specific discharge capacity than the SL porous due to the binder migration that occurs. With an increase in specific capacity at 3 C of 67% compared to the single layer with compact particles, the multilayer ML 1/3 porous shows a

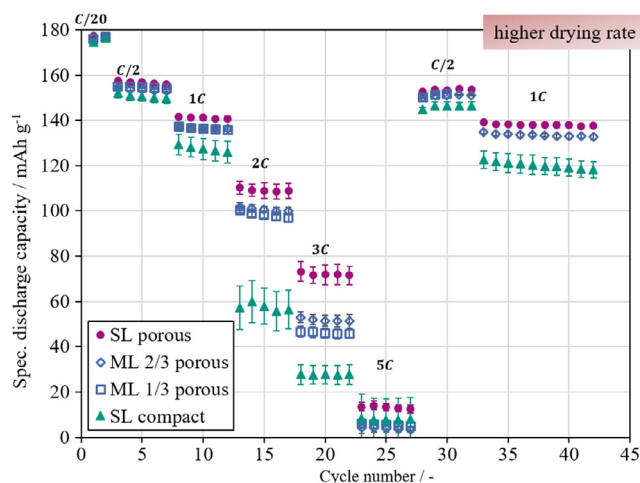


Figure 7. Specific discharge capacities of half cells with non-calendered single-layer (SL compact: green triangles, SL porous: red dots) and multi-layer electrodes (ML 1/3 porous: blue squares, ML 2/3 porous: blue rhombus) at a constant drying rate of $2.25 \text{ g m}^{-2} \text{ s}^{-1}$.

lower increase in C-rate capability at a higher drying rate than the ML 2/3 porous. This could be related to the lower proportion of porous particles.

Compared to the lower drying rate, a reduction in specific discharge capacity is shown for SL porous for 2 and 3 C of 4% and 9%, respectively. This confirms that electrodes with porous particles also show binder migration, but the negative effects on electrochemical performance are significantly reduced.^[1] The findings from the studies on the adhesion force and resistivity support that if the total binder content decreases, the properties of the electrodes suffer relatively more at increasing drying rate. This can be partially confirmed by the cell tests. The electrodes show a reduction in specific capacity at a discharge rate of 3 C compared to electrodes dried at a lower drying rate of 23% (SL compact, 4.5 wt% PVDF), 32% (ML 1/3 porous, 4 wt% PVDF), and 28% (ML 2/3 porous, 3.5 wt% PVDF). Focusing alone on the overall binder content, it would have been expected that the multilayer ML 2/3 porous would have a lower specific capacity at higher drying rates. The deviation may be related to the superposition of the influences of the overall binder content and the higher share of the porous particles.

3. Conclusion

In this work, multilayer electrodes were produced simultaneously with compact and porous, nanostructured particles to optimize the electrode properties. The multilayer configuration was supposed to improve the adhesion force compared to a single layer with only porous particles, and the C-rate capability compared to a single layer with only compact particles. Thereby, the focus was to investigate the influence of drying on the electrode properties.

For the multilayer electrodes, different layer configurations were produced with different proportions of porous particles and with a reduced binder content in the top layer of the coating.

The multilayer electrodes (ML 1/3 porous and ML 2/3 porous) show a higher adhesion force than the single-layer electrodes with porous material (SL porous) at lower and higher drying rate, respectively. The multilayer electrode, which consists of 2/3 compact particles (ML 1/3 porous) toward the separator side, shows a 16-times higher adhesion force at the lower drying rate and a 10-times higher adhesion force at the higher drying rate – more oriented towards the adhesion force of the single-layer electrode with compact particles. It has been shown by half-cell tests that despite binder migration is occurring during drying with the higher drying rate, the C-rate capability of the multilayer and single-layer electrode with porous particles was increased compared to the single layer with compact particles. Compared to the single-layer electrode with compact particles, the multilayer electrode with a higher proportion of porous particles shows an increase in specific discharge capacity of 88% and of 67%, respectively, at the higher drying rate and a discharge rate of 3 C. For increasing drying rate, all investigated electrodes show a decrease in adhesion force, C-rate capability and an increase in resistivity. In particular, it was found that for the formulations and coating configurations used, the adhesion force correlates with the overall binder content of the electrodes.

The findings show that a selectively accessible porosity and the overall binder content influence the binder migration during the drying of multilayer electrodes. However, a mechanistic understanding of the drying and binder migration of multilayer electrodes with the PVDF/NMP binder/solvent system is necessary for further optimization of electrode properties, as it is still a widespread binder-solvent system for NMC cathodes. Nevertheless, future studies will also investigate the processing of aqueous cathodes with different particle morphology in single-layer and for multilayer architectures at increasing drying rates.

4. Experimental Section

Slurry Materials and Cathode Mixing: Active Material Characterization: The specific surface was obtained by BET measurement using nitrogen adsorption gas (Gemini VII 2390, Micromeritics). The densities of the materials were measured by helium pycnometry (AccuPyc 1330, Porotec).

Slurry Materials and Cathode Mixing: Mixing: The slurry for NCM622-compact (NCM622, BASF) and NCM622-porous cathodes were mixed in a dissolver (Dispermat SN-10, VMA Getzmann/Germany). The conductive additives carbon black (C-Nergy Super C65, Imerys) and graphite (C-ENERGY KS6L, Imerys), a PVDF (Solef 5130, Solvay) binder-solvent solution (7.5 wt%) and about 50% of the required amount of NMP (Carl Roth) were dispersed at 1000 rpm for 30 min. The active material and the remaining NMP were added to adjust the solid content (55 wt%) and dispersed at 1000 rpm for further 30 min. The compositions of the dry electrodes are shown in **Table 3**. The viscosity was measured by a rotational viscometer (Physica MCR 101, Anton Paar) in a plate-plate system with 25 mm diameter measuring head from 0.1 to 1500 s⁻¹ at 25 °C. Before starting the measurement, the sample was sheared at 0.1 s⁻¹ for 60 s.

Table 3. Composition of the dry electrodes with NCM622-compact and NCM622-porous.

Name	NCM [wt%]	KS6L [wt%]	C65 [wt%]	PVDF [wt%]	Solids [wt%]
NCM622-compact	90.5	2.0	3.0	4.5	55
NCM622-porous	92.0	2.0	3.0	3.0	55

Cathode Coating and Drying: The coating and drying of the single-layer or multilayer-cathode electrodes was carried out as a discontinuous process. The aluminum foil (Schlenk, 20 μm) was attached to a temperature-controlled plate. The coating of the cathode slurries was applied by a doctor blade (ZUA 2000.60, Zehntner) and subsequently the coating was moved under the drying nozzles of an impingement dryer. For homogeneous drying, the coating was moved periodically under the dryer.

Electrodes Characterization: Porosity: The porosity of the electrodes was calculated with the area weight $m_{\text{electrode}}$ divided by the density of the dry mixture $\rho_{\text{dry mixture}}$ and the dry electrode thickness h_{dry} (Equation (1)).

$$\epsilon_{\text{electrode}} = 1 - \frac{m_{\text{electrode}}}{\rho_{\text{dry mixture}} \cdot h_{\text{dry}}} \quad (1)$$

The density of the dry mixture was calculated using Equation (2) with the mass fractions in the dry electrode and the densities of the components. ρ_{NCM} is the density from Table 1, measured by helium pycnometry.

$$\rho_{\text{dry mixture}} = \left(\frac{x_{\text{NCM}}}{\rho_{\text{NCM}}} + \frac{x_{\text{C65}}}{\rho_{\text{C65}}} + \frac{x_{\text{KS6L}}}{\rho_{\text{KS6L}}} + \frac{x_{\text{PVDF}}}{\rho_{\text{PVDF}}} \right)^{-1} \quad (2)$$

To calculate the interparticle porosity, the envelope density according to Equation (3) is used instead of the density in Equation (2).

$$\rho_{\text{envelope}} = \rho_{\text{NCM622-porous}} (1 - \epsilon_{\text{open particle porosity}}) \quad (3)$$

Electrodes Characterization: Adhesion: To determine the adhesion force of the electrode coating on the substrate, a 90° peel test was carried out (10 N load cell, Zwick). Sample strips of the dried cathodes were cut out with a width of 17 mm, attached with the coated side to an adhesive strip, and exposed to a weight of 200 kg using an MP150D hand press (Maassen). The current collector foil was then peeled off the coating at a constant speed of 600 mm min⁻¹ at a 90° angle using the testing machine. The resulting pull-off force was measured and divided by the sample width to obtain the line force.

Electrodes Characterization: Resistivity: The resistivity was determined with an ohmmeter (HIOKI, RM3544). For this purpose, circular samples of the cathodes were placed between polished copper cylinders with a diameter of 14 mm and pressed by a force of 9.81 N.

Electrodes Characterization: SEM: A Zeiss Supra 55 from Carl Zeiss AG (Oberkochen, Germany) was used for SEM investigations.

Half-Cell Preparation and Cell Test: The cathodes (13 mm) were electrochemically examined in CR2032 coin cells against a lithium-metal (16 mm) counter electrode. The electrolyte used was 200 μL of LP30 (BASF) with the conductive salt 1 M LiPF₆ in an EC/DMC (1:1) mixture. The two separators made of a glass-microfiber fleece (GF/C, Whatman) had a diameter of 16 mm. The cells were assembled in an argon filled glovebox and sealed with a MSK-11 press (MTI, KJ Group).

The cycling was carried out in a BT2000 battery cyler (Arbin Instruments) in constant current mode inside a voltage range of 3–4.3 V. Identical C-rates were used for charging and discharging. After two formation cycles at a C-rate of C/20, the C-rate was gradually increased up to 5 C. Then additional steps were carried out at C/2 and 1 C. The standard deviation between different electrodes and different coin cells is given.

Supporting Information

Supporting Information is available from the Wiley Online Library or from the author.

Acknowledgements

This work contributes to the research performed at CELEST (Center for Electrochemical Energy Storage Ulm Karlsruhe) and Material Research Center for Energy Systems (MZE). It was funded by the Deutsche Forschungsgemeinschaft (DFG, German Research Foundation) under

Germany's Excellence Strategy – EXC 2154 – Project number 390874152 (POLiS Cluster of Excellence). The authors would like to thank the assistants involved in this work.

Open Access funding enabled and organized by Projekt DEAL.

Conflict of Interest

The authors declare no conflict of interest.

Data Availability Statement

The data that support the findings of this study are available from the corresponding author upon reasonable request.

Keywords

binder migration, electrode processing, hierarchical structured materials, lithium-ion batteries, microstructure optimizations, multilayer electrodes, NCM

Received: March 15, 2023

Revised: May 5, 2023

Published online:

- [1] J. Klemens, L. Schneider, E. C. Herbst, N. Bohn, M. Müller, W. Bauer, P. Scharfer, W. Schabel, *Energy Technol.* **2022**, 2100985.
- [2] A. C. Wagner, N. Bohn, H. Geßwein, M. Neumann, M. Osenberg, A. Hilger, I. Manke, V. Schmidt, J. R. Binder, *ACS Appl. Energy Mater.* **2020**, 3, 12565.
- [3] M. Müller, L. Schneider, N. Bohn, J. R. Binder, W. Bauer, *ACS Appl. Energy Mater.* **2021**, 4, 1993.
- [4] J. Landesfeind, H. A. Gasteiger, *J. Electrochem. Soc.* **2019**, 166, A3079.
- [5] S. Hein, T. Danner, D. Westhoff, B. Prifling, R. Scurtu, L. Kremer, A. Hoffmann, A. Hilger, M. Osenberg, I. Manke et al., *J. Electrochem. Soc.* **2020**, 167, 13546.
- [6] X. Li, J. Liu, M. N. Bani, A. Lushington, R. Li, M. Cai, X. Sun, *Energy Environ. Sci.* **2014**, 7, 768.
- [7] L. Schneider, J. Klemens, E. C. Herbst, M. Müller, P. Scharfer, W. Schabel, W. Bauer, H. Ehrenberg, *J. Electrochem. Soc.* **2022**, 169, 100553.
- [8] T. Akçay, M. Häring, K. Pfeifer, J. Anhalt, J. R. Binder, S. Dsoke, D. Kramer, R. Mönig, *ACS Appl. Energy Mater.* **2021**, 4, 12688.
- [9] A. H. Salehi, S. M. Masoudpanah, M. Hasheminasari, A. Yaghtin, D. Safanama, C. K. Ong, S. Adams, K. Zaghbi, M. V. Reddy, *J. Power Sources* **2021**, 481, 228828.
- [10] W. Zheng, X. Huang, Y. Ren, H. Wang, S. Zhou, Y. Chen, X. Ding, T. Zhou, *Solid State Ionics* **2017**, 308, 161.
- [11] I. U. Mohsin, L. Schneider, M. Häring, C. Ziebert, M. Rohde, W. Bauer, H. Ehrenberg, H. J. Seifert, *J. Power Sources* **2022**, 545, 231901.
- [12] M. Baunach, S. Jaiser, S. Schmelzle, H. Nirschl, P. Scharfer, W. Schabel, *Dry. Technol.* **2016**, 34, 462.
- [13] R. Diehm, J. Kumberg, C. Dörrer, M. Müller, W. Bauer, P. Scharfer, W. Schabel, *Energy Technol.* **2020**, 8, 1901251.
- [14] H. Hagiwara, W. J. Suszynski, L. F. Francis, *J. Coat. Technol. Res.* **2014**, 11, 11.
- [15] S. Jaiser, L. Funk, M. Baunach, P. Scharfer, W. Schabel, *J. Colloid Interface Sci.* **2017**, 494, 22.
- [16] S. Jaiser, J. Kumberg, J. Klaver, J. L. Urai, W. Schabel, J. Schmatz, P. Scharfer, *J. Power Sources* **2017**, 345, 97.
- [17] S. Jaiser, M. Müller, M. Baunach, W. Bauer, P. Scharfer, W. Schabel, *J. Power Sources* **2016**, 318, 210.
- [18] S. Jaiser, N. Sanchez Salach, M. Baunach, P. Scharfer, W. Schabel, *Dry. Technol.* **2017**, 35, 1807.
- [19] J. Kumberg, W. Bauer, J. Schmatz, R. Diehm, M. Tönsmann, M. Müller, K. Ly, P. Scharfer, W. Schabel, *Energy Technol.* **2021**.
- [20] J. Kumberg, M. Baunach, J. C. Eser, A. Altvater, P. Scharfer, W. Schabel, *Energy Technol.* **2021**, 9, 2100013.
- [21] J. Kumberg, M. Müller, R. Diehm, S. Spiegel, C. Wachsmann, W. Bauer, P. Scharfer, W. Schabel, *Energy Technol.* **2019**, 7, 1900722.
- [22] S. Lim, K. H. Ahn, M. Yamamura, *Langmuir* **2013**, 29, 8233.
- [23] R. Morasch, J. Landesfeind, B. Suthar, H. A. Gasteiger, *J. Electrochem. Soc.* **2018**, 165, A3459.
- [24] M. Müller, L. Pfaffmann, S. Jaiser, M. Baunach, V. Trouillet, F. Scheiba, P. Scharfer, W. Schabel, W. Bauer, *J. Power Sources* **2017**, 340, 1.
- [25] B. Westphal, H. Bockholt, T. Gunther, W. Haselrieder, A. Kwade, *ECS Trans.* **2015**, 64, 57.
- [26] B. G. Westphal, A. Kwade, *J. Energy Storage* **2018**, 18, 509.
- [27] J. Landesfeind, A. Eldiven, H. A. Gasteiger, *J. Electrochem. Soc.* **2018**, 165, A1122.
- [28] J. Landesfeind, M. Ebner, A. Eldiven, V. Wood, H. A. Gasteiger, *J. Electrochem. Soc.* **2018**, 165, A469.
- [29] A. Altvater, T. Heckmann, J. C. Eser, S. Spiegel, P. Scharfer, W. Schabel, *Energy Technol.* **2022**, 2200785.
- [30] J. Yang, Y. Li, A. Mijailovic, G. Wang, J. Xiong, K. Mathew, W. Lu, B. W. Sheldon, Q. Wu, *J. Mater. Chem. A* **2022**, 10, 12114.
- [31] Y. Dai, V. Srinivasan, *J. Electrochem. Soc.* **2016**, 163, A406.
- [32] L. Neidhart, K. Fröhlich, N. Eshraghi, D. Cupid, F. Winter, M. Jahn, *Nanomaterials* **2022**, 12, 317.
- [33] R. Diehm, M. Müller, D. Burger, J. Kumberg, S. Spiegel, W. Bauer, P. Scharfer, W. Schabel, *Energy Technol.* **2020**, 8, 2000259.
- [34] D. Liu, L.-C. Chen, T.-J. Liu, W.-B. Chu, C. Tiu, *Energy Technol.* **2017**, 5, 1235.
- [35] L.-C. Chen, D. Liu, T.-J. Liu, C. Tiu, C.-R. Yang, W.-B. Chu, C.-C. Wan, *J. Energy Storage* **2016**, 5, 156.
- [36] W. S. Schabel, P. S. Scharfer, M. K. Kind, *Chem. Ingen. Tech.* **2003**, 75, 1105.
- [37] J. C. Eser, B. Deichmann, T. Wirsching, L. Merklein, M. Müller, P. Scharfer, W. Schabel, *Dry. Technol.* **2022**, 40, 1130.